

A Data-Driven Framework for Discovering Fractional Differential Equations in Complex Systems

Xiangnan Yu^a, Hao Xu^a, Zhiping Mao^a, HongGuang Sun^c, Yong Zhang^d, Dongxiao Zhang^{a,b}, Yuntian Chen^{a,b,*}

^aEastern Institute of Technology, Ningbo, Zhejiang 315200, People's Republic of China

^bZhejiang Key Laboratory of Industrial Intelligence and Digital Twin, Eastern Institute of Technology, Ningbo, Zhejiang 315200, China

^cInstitute of Hydraulics and Fluid Mechanics, Hohai University, Nanjing 211100, China.

^dDepartment of Geological Sciences, University of Alabama, Tuscaloosa, AL, USA.

Abstract

In complex physical systems, conventional differential equations often fall short in capturing non-local and memory effects, as they are limited to local dynamics and integer-order interactions. This study introduces a stepwise data-driven framework for discovering fractional differential equations (FDEs) directly from data. FDEs, known for their capacity to model non-local dynamics with fewer parameters than integer-order derivatives, can represent complex systems with long-range interactions. Our framework applies deep neural networks as surrogate models for denoising and reconstructing sparse and noisy observations while using Gaussian-Jacobi quadrature to handle the challenges posed by singularities in fractional derivatives. To optimize both the sparse coefficients and fractional order, we employ an alternating optimization approach that combines sparse regression with global optimization techniques. We validate the framework across various datasets, including synthetic anomalous diffusion data, experimental data on the creep behavior of frozen soils, and single-particle trajectories modeled by Lévy motion. Results demonstrate the framework's robustness in identifying the structure of FDEs across diverse noise levels and its capacity to capture integer-order dynamics, offering a flexible approach for modeling memory effects in complex systems.

Keywords: Fractional differential equations; Knowledge discovery; Sparse regression; Gaussian-Jacobi quadrature; Machine learning.

1. Introduction

Differential equations, typically derived from fundamental physical principles, are important for modeling physical phenomena. However, progress in developing these differential models is often hindered by limited physical intuition and mathematical expertise. Advancing in data acquisition and storage capabilities have created new opportunities for deriving differential equations through data-driven methodologies [1]. The data-driven discovery approach aims to automatically extract the governing equations from data without prior knowledge.

A pioneering method in this field is symbolic regression [2], which uses an evolutionary algorithm to find optimal combinations of coefficients and candidate analytical equations, balancing model simplicity with accuracy. Based on symbolic regression, Bongard and Lipson [3] introduced a technique to learn coupled nonlinear ordinary equations directly from time series, while Schmidt and Lipson [4] expanded this to derive conservation laws in dynamic systems from motion-tracking data. Sparse regression is another important framework for identifying structural forms of differential equations, Brunton et al. [5] proposed the SINDy framework, a sparse regression method for deriving the governing equation from noisy data, particularly, through dimensionality reduction for partial differential equation extraction. However, SINDy struggles with high-dimensional data, limiting its applicability, as many experiments collect observations in high-dimensional space (e.g., tracer concentration time-series at various locations in dispersive transport studies). Rudy et al. [6] extended SINDy to handle spatio-temporal synthetic data via STRidge, a sequential

* Author for correspondence. Email-address: ychen@eitech.edu.cn (Yuntian Chen)

threshold ridge regression approach that constructs a candidate library of time and space derivatives and employs sparse regression with l_0 -regularization. Chang and Zhang [7] developed a framework using the least absolute shrinkage and selection operator (LASSO) to learn subsurface flow equations, though both STRidge and LASSO rely highly on accurate numerical derivative approximations, making them sensitive to data sparsity and measurement noise. To address these challenges, Messenger and Bortz [8] extended SINDy to WSINDy by applying a convolutional weak formulation, successfully uncovering PDEs from noisy data. Fasel et al. [9] applied statistical methods to enhance SINDy’s robustness with sparse, and noisy data subsets. Particularly, deep neural networks (DNNs) have been recognized as an effective approach for mitigating data noise and sparsity. DNNs serve as surrogates for the sparse and noisy data, producing reconstructed data with diminished noise and enhanced resolution. For instance, Xu et al. [10] combined DNNs and STRidge to discover conventional PDEs under noisy and sparse data, the proposed method achieves better result than original STRidge. Both et al. [11] proposed a deep learning-based LASSO to enhance the robustness in model discovery with noisy, sparse data. Raissi et al. [12] introduced physics-informed neural networks (PINNs) to study both the forward and inverse problems of PDEs under sparse and noisy data conditions, though this method requires prior knowledge of PDE structure. It is important to note that studies on discovering governing equations can be broadly categorized into two types: structure discovery and coefficients discovery [13], PINNs belongs to latter one. Xu and Zhang [14] proposed the R-DLGA framework, which combines PINNs with genetic algorithm to enable the structure discovery of PDEs, and achieve to withstand noise levels up to 50%.

However, the frameworks mentioned above are limited to recovering basic governing equations in simple system. In contrast, natural systems are typically complex, characterized by multiscale physics and anomalous phenomena. For example, dispersive transport in heterogeneous porous media show anomalous dispersion, characterized by non-Gaussian spatial concentration distribution or nonlinear mean squared displacement growth [15, 16]. To capture anomalous phenomena, an alternative method is direct modeling through tradition models with time- and space-variable parameters [17], i.e., using advection-dispersion equation with fine-resolution hydraulic conductivity fields to capture solute transport in heterogeneous media [18, 19]. Note that it requires detailed parameterization on aquifer heterogeneity, which pose significant challenges for aforementioned data-driven discovery approaches. To derive parametric PDEs without prior knowledge, a more advanced model discovery algorithm is needed. Rudy et al. [17] enhanced STRidge to group STRidge, showing it outperforms other discovery framework for parametric PDEs. Xu et al. [20] used integral forms of PDEs to mitigate noise, achieving PDEs identification with heterogeneous parameters. Chen et al. [21] proposed SGA-PDE, which combined symbolic regression with genetic algorithm to achieve the flexible representation of any parametric PDE. Additionally, SGA-PDE is an open-form equation discovery framework, i.e., it does not rely on the overcomplete, closed candidate library. Du et al. [22] integrated reinforcement learning into the SGA-PDE framework to improve the accuracy and efficiency of discovering PDEs with fractional structure (i.e., variable fraction parameter) and higher-order derivatives. Furthermore, they introduced a robust version of the framework to handle highly noisy data [23] and proposed a Large Language Model (LLM)-guided equation discovery framework to break through the barriers to interdisciplinary research [24].

Nevertheless, challenges remain: first, identifying heterogeneous parameters is time-intensive due to the large number of coefficients [25]. second, issues such as mathematical ill-posed problem and parameter equifinality, where different parameter sets yields similar transport behaviors [26], complicate inverse modeling and can lead to incorrect models. Current approaches are limited to discovering PDEs with weakly varying parameters [13]. In natural systems, however, parameters often exhibit multiscale variability and may change significantly across both time and space, as seen in hydraulic conductivity fields in aquifers [27]. Consequently, the applicability of current model discovery methods remains constrained in the context of highly complex systems.

An intrinsic approach for reducing the difficulty of model discovery in highly complex systems is model upscaling, which reduces the degrees of freedom in the equations and the number of parameters using techniques such as mathematical homogenization or stochastic methods [28]. The representative application applying upscaling tools is dispersive transport in aquifers, various parsimonious (upscaled) models have been developed to capture macroscopic transport in aquifers [29, 28], including the stochastic average advection model [30], continuous-time random walks [31], fractional advection-diffusion equations [32], and the multi-rate mass transfer model [33]. These models effectively capture dispersive transport in highly heterogeneous media with only a few additional parameters, significantly reducing the degrees of freedom and parameters of equations. Although several data-driven techniques have been proposed for upscaling or discovering upscaled models [34, 35, 36], the development of methods for uncovering models that describe the dynamics of complex environments, such as anomalous diffusion in heterogeneous media, remains

to be explored. Among the upscaled models mentioned above, fractional advection-diffusion equations are especially promising due to the well-studied mathematics of fractional calculus [37, 38, 39] and various numerical algorithms [40]. Beyond geology, fractional differential equations (FDEs) have been widely applied to model non-local dynamics in complex systems over the past several decades [41], including anomalous diffusion [15], non-Newtonian fluids [42], creep and relaxation [43] and continuous finance [44], among others. Promoting the development of models that incorporate fractional calculus remains a significant effort [41]. Data-driven discovery of FDEs is essential to accelerate this development, which motivate this study. However, discovering FDEs presents computational challenges. Firstly, the singular nature of the power-law kernel function affects the accuracy and stability of solution [45]. Secondly, the nonlocality of convolution, with interactions over distance or time, necessitates the computation of fractional derivatives using the values of functions at multiple nonlocal nodes. Thirdly, current sparse regression methods can only optimize the coefficients linearly multiply the candidate derivative terms, limiting their ability to adjust fractional order.

In this study, we propose a stepwise framework for discovering FDEs that effectively addresses these challenges. This framework uses Gaussian-Jacobi quadrature to overcome the singularity of the power-law kernel [45] and to provide high-accuracy approximations for fractional derivatives [46]. A deep learning-based surrogate model reconstructs noisy and sparse data, achieving denoising and super-resolution. Additionally, automatic differentiation within deep neural networks enables the computation of integer-order derivatives in machine precision at arbitrary positions, facilitating the use of Gaussian-Jacobi quadrature to build a complete library of candidate terms, including fractional derivatives. Sparse coefficients and fractional orders are optimized alternately using sparse regression and global optimization algorithms.

The remainder of this work is organized as follows: Section 2 presents the FDE discovery framework, including definitions of fractional calculus and the stepwise method for discovering FDEs, Section 3 demonstrates the effectiveness of the proposed algorithm through various FDE discoveries, and Section 4 discusses the characteristics of our method. Finally, Section 5 summarizes conclusions and directions for future work.

2. FDE discovery framework

2.1. Fractional differential equation

We consider a general form of a partial differential equation extended by incorporating fractional derivatives as follows:

$$u_t^{(\alpha)} = \mathcal{F}(u, u_x, u_x^{(\beta)}, u_{xx}, \dots) \xi, \quad (1)$$

where the subscripts t and x denote the derivative of function u with respect to time and space. The superscripts " (α) " and " (β) " denote the fractional order of differentiation in time and space, $\mathcal{F}(\cdot)$ is a linear operator to be found, formed by the linear combination of the coefficient vector ξ and the various derivatives of u .

In engineering fields, fractional calculus is commonly defined in two forms: the Riemann-Liouville (R-L) definition and the Caputo definition. The R-L derivative is expressed as

$$u_x^{(\gamma)} = {}_{-\infty}^{RL}D_x^\gamma u(x) = \frac{d^n}{dx^n} I^{n-\gamma} u(x), \quad (2)$$

and the Caputo derivative is given by

$$u_t^{(\gamma)} = {}_0^C D_t^\gamma u(t) = I^{n-\gamma} \frac{d^n u(t)}{dt^n}, \quad (3)$$

where I^γ denotes the γ -th (arbitrary real number) order of fractional integrals,

$$I_a^\gamma u(t) = \frac{1}{\Gamma(\gamma)} \int_a^t (t-\tau)^{\gamma-1} u(\tau) d\tau, \quad (4)$$

and n represents the integer obtained by rounding up the value of α . For fractional derivatives with respect to time, the Caputo definition is commonly used because it provides reasonable initial conditions [38]. Conversely, space fractional derivatives are often defined by the R-L definition, given the common assumption of an infinite computational domain. There is a relationship between the two definitions:

$${}_a^C D_x^\gamma u(x) = {}_a^{RL} D_x^\gamma u(x) - \sum_{i=0}^{n-1} \frac{(x-a)^{i-\gamma}}{\Gamma(i-\gamma+1)} u^{(i)}(a) \quad (5)$$

where a denotes the initial node, and i represents the integer order of the derivative. As shown in Equation (5), when the computational region is sufficiently large and boundary conditions are minimal, which is common in natural systems, the R-L derivative can be approximated by the Caputo derivative [37].

2.2. Sparse regression

Assuming that the function \mathcal{F} (see Equation (1)) is composed of a linear multiplication of coefficients and candidate derivative terms, Equation (1) can be discretized as

$$\mathbf{u}_t^{(\alpha)} = \Theta(\beta) \cdot \boldsymbol{\xi}, \quad (6)$$

where Θ denotes the candidate library, containing all possible (linear or nonlinear) terms including fractional order β with respect to space, expressed as

$$\Theta(\beta) = \begin{pmatrix} 1 & u(x_1, t_1) & \cdots & u_x^{(\beta)}(x_1, t_1) & \cdots \\ 1 & u(x_2, t_1) & \cdots & u_x^{(\beta)}(x_2, t_1) & \cdots \\ \vdots & \vdots & \ddots & \vdots & \ddots \\ 1 & u(x_M, t_1) & \cdots & u_x^{(\beta)}(x_M, t_1) & \cdots \\ \vdots & \vdots & \ddots & \vdots & \ddots \\ 1 & u(x_M, t_N) & \cdots & u_x^{(\beta)}(x_M, t_N) & \cdots \end{pmatrix}, \quad (7)$$

Θ and $\mathbf{u}_t^{(\alpha)}$ should be calculated prior to solving the learning problem, which involves evaluating the sparse coefficient vector $\boldsymbol{\xi}$. The primary objective of this study is to determine α , β and $\boldsymbol{\xi}$ by solving the following regression problem:

$$(\hat{\boldsymbol{\xi}}, \hat{\alpha}, \hat{\beta}) = \arg \min_{(\boldsymbol{\xi}, \alpha, \beta)} \left(\|\mathbf{u}_t^{(\alpha)} - \Theta(\beta) \cdot \boldsymbol{\xi}\|_2^2 + \lambda \|\boldsymbol{\xi}\|_2^2 \right), \quad (8)$$

where λ denotes the regularization parameter, which is crucial for balancing parsimony and accuracy in the governing function.

2.3. Generating the library of candidate derivative terms

The elements in Equation (7) should be predefined, with integer-order derivatives conveniently computed using automatic differentiation. While generating fractional derivative terms is complex. Calculating fractional-order derivatives requires function values from both local and nonlocal regions due to the inherent nonlocality in their definitions: as demonstrated in Equations (2) and (3), where the convolution integrals extend from the origin to distant regions. Moreover, data sparsity and noise complicate the calculation of derivative terms. To address these challenges, we employ deep neural networks (DNN) to simultaneously denoise and perform super-resolution reconstruction of sparse data fields. DNN serves as a surrogate model, with its capabilities of data interpolation and noise smoothing, making it well-suited for handling sparse and noisy data. Moreover, the automatic differentiation embedded in DNN can calculate the integer-order derivative component in fractional derivatives in high precision and robustness. The dataset is processed with a DNN as follows:

$$u(\mathbf{z}) \approx \hat{u}(\mathbf{z}) = y_n(y_{n-1}(\dots(y_2(\mathbf{z}))))), \quad (9)$$

where $u(\mathbf{z})$ and $\hat{u}(\mathbf{z})$ denote the original dataset and reconstructed data, respectively, $\mathbf{z} = (x, y, z, t)$ is the coordinate vector in space and time, and

$$y_i(\mathbf{z}) = \sigma(\boldsymbol{\omega}_i \mathbf{z} + \mathbf{b}_i), i = 1, 2, \dots, n, \quad (10)$$

where n denotes the number of hidden layers, σ is the chosen activation function, and ω_i and \mathbf{b}_i represent the weights and bias in i th layer, respectively. The cost function for the DNN is defined as

$$\mathcal{L}(z, \omega) = \frac{1}{N} \sum_{i=1}^N (\hat{u}(z_i) - u(z_i))^2 + \lambda \|\omega\|^2, \quad (11)$$

where N denotes the number of measurements. The loss function \mathcal{L} is used to train the DNN, and the regularization term $\lambda \|\omega\|^2$ helps prevent overfitting the noisy data, where the hyperparameter λ controls the trade-off between fitting the training set and validation set. Once a high-quality reconstructed data field is created, the integer-derivative terms can be analytically estimated within the DNN by applying auto-differentiation. However, fractional derivative terms can not be generated solely through automatic differentiation of the DNN solution $\hat{u}(\mathbf{z})$. Mesh-based methods, such as the finite difference method and the Grünwald-Letnikov difference scheme, have been used to obtain fractional derivatives within the deep learning framework, as in the previous work [47]. However, mesh methods can suffer from singularity issues that affect accuracy and stability for approximating fractional derivatives, and their global nature requires numerous equidistant auxiliary points from origin, leading to high computational cost at large scales. As an alternative, we introduce the Gaussian-Jacobi (G-J) quadrature approach, which uses orthogonal polynomials to provide a high-accuracy approximation of fractional integrals through coordinate transformation (see Appendix A). According to Equations (2) and (3), fractional derivatives combine integer-order derivatives and fractional integrals. Thus, by integrating auto-differentiations in deep learning framework such as PyTorch into the Gaussian-Jacobi quadrature, fractional derivative terms can be efficiently computed in a fixed number of auxiliary nodes (generated by DNN). The procedure for generating fractional derivatives (e.g., in time at $t = t_i$) is summarized as follows: first, initialize the input and calculate approximate integer derivative component using automatic differentiation. Second, rewrite the formulation of the fractional derivative

$$\hat{u}_t^{(\alpha)}(x, t) \Big|_{t=t_i} = \frac{\partial^\alpha \hat{u}(x, t) \Big|_{t=t_i}}{\partial t^\alpha} = \frac{1}{\Gamma(n-\alpha)} \int_0^{t_i} \tau^{n-1-\alpha} \frac{\partial^n \hat{u}(x, t) \Big|_{t=t_i-\tau}}{\partial t^n} d\tau \quad (12)$$

to match the G-J quadrature via the variable transformation $\tau = t_i(1 + \zeta)/2$, we obtain

$$\hat{u}_t^{(\alpha)}(x, t) \Big|_{t=t_i} = \frac{(t_i/2)^{n-\alpha}}{\Gamma(n-\alpha)} \int_{-1}^1 (1 + \zeta)^{n-1-\alpha} \frac{\partial^n \hat{u}(x, t) \Big|_{t=\frac{t_i}{2}(1-\zeta)}}{\partial t^n} d\zeta. \quad (13)$$

The calculation of derivative terms can be treated as an algebraic equation with a fixed number of terms, as shown in Equations (A.1) and (A.2). In this study, we select five quadrature nodes; while more nodes can improve accuracy, five nodes generally offer a good balance between computational efficiency and accuracy. Fractional derivatives in terms of space follow the same process. The G-J quadrature outperforms mesh methods (e.g., finite difference method) as it requires only a few auxiliary nodes. Numerical examples are provided in Appendix A. The workflow for generating the library of derivative terms is outlined below (Figure 1).

2.4. Stepwise optimization approach

According to Equation (8), the cost function comprised of the mean squared error (MSE) related to the sparse vector ξ , fractional orders α and β , and a regularization term, formulated as follows

$$\mathcal{L}(\alpha, \beta, \xi) = \left\| u_t^{(\alpha)} - \Theta(\beta) \cdot \xi \right\|_2^2 + \lambda \|\xi\|_2^2. \quad (14)$$

To extract the structural form of integer-order differential equations, sparse regression algorithms such as STRidge [6] have proven effective and are integrated into various advanced PDE discovery frameworks [10, 48]. However, applying the sparse regression to discover FDEs poses challenges due to the nonlocal nature of fractional derivatives. The STRidge algorithm identifies a sparse coefficient vector ξ that linearly multiplies prescribed derivative terms, but cannot estimate the fractional order, a continuously latent parameter [49] hidden within the candidate library rather than represented by sparse coefficients. [50] proposed a framework using two DNNs to capture physical dynamics, effectively avoiding issues with latent parameters. However, the resulting model is a black-box, lacking a closed-form governing equation. The black-box nature hinders researchers to further study the theoretical properties of governing equations.

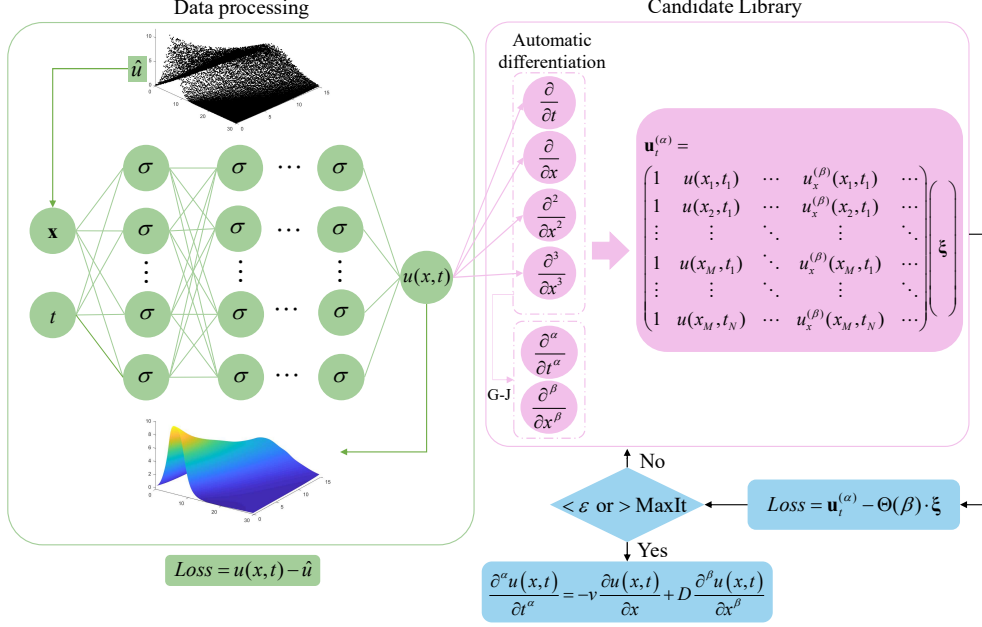


Figure 1: Workflow for data processing and generating the library of derivative terms.

To obtain both the optimal fractional order and sparse coefficients, we design an alternating optimization approach that estimates the sparse coefficients vector and fractional order sequentially, see Figure 2a. Sparse coefficients are obtained by STRidge, while the fractional order is estimated using a global optimization algorithm, as the loss function (14) is non-convex and discontinuous due to the discontinuity of the l_0 -regularization, where the number of non-zero terms is an integer and changes discontinuously during optimization (see Figure 2b for details). In such cases, gradient-based optimization algorithms, such as the Adam algorithm and Newton's iterative methods, may encounter ill-posed problems at the discontinuous interface of the loss function. After our practical tests, Simulated Annealing (SA), Differential Evolution (DE), and Particle Swarm Optimization (PSO) proved viable for this task, with DE identified as the most effective due to its stability, robustness and rapid convergence capabilities. Therefore, DE was used to estimate the fractional order in this study. The optimization procedure consists of the following steps (see Table 1).

3. Results

In this section, we validate the applicability of our method for identifying fractional differential equations directly from data, without requiring prior knowledge of the equation structure. We present a series of case studies, including synthetic data for the fractional advection-diffusion equation, experimental data on the creep process of frozen soils, and time-series data from single particle tracking that conforms to an α -stable distribution. Initially, we consider a straightforward case study involving experimental data that is described by a fractional ODE. The experimental data for this scenario is relatively straightforward to obtain.

3.1. Discovering the fractional Kelvin model from experimental data

We examine the uniaxial compression creep of frozen soil as a case study. This creep process is complex, influenced by mechanical properties that include multiphase components and various environmental conditions. Tradi-

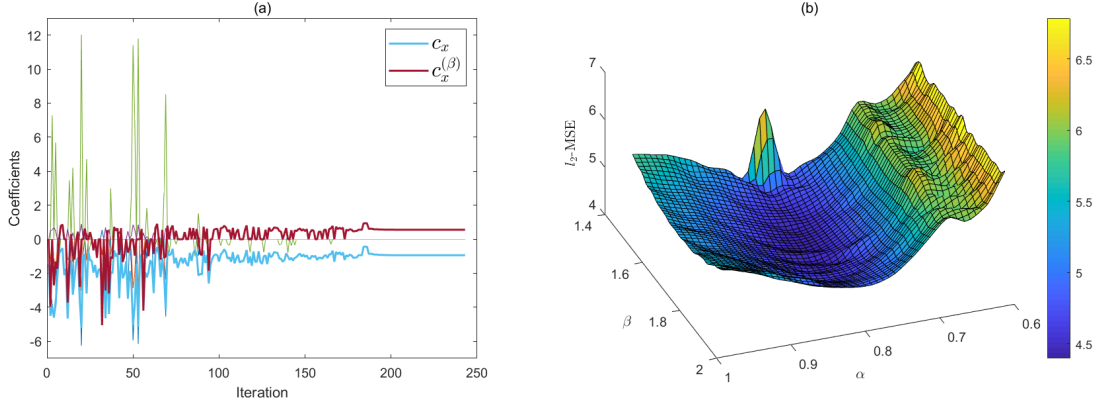


Figure 2: (a) Evolution of sparse coefficients estimated via our alternating optimization approach, y-coordinate represents the best sparse coefficients ξ estimated by STRidge under fixed fractional orders, x-coordinate represents the iterations of global optimization algorithm. (b) Evolution of loss function (14) with fractional orders. The specific example presented in this figure involves a fractional advection-diffusion equation with incorporates a 5% uniform noise in Section 3.2.

tionally, it has been modeled using ordinary differential equations (ODEs) to describe stress-strain relationships and incorporate the memory effects. Studies show that fractional constitutive models better capture the time-dependent behavior and memory effects in the creep process [43]. Here, we applied our method to derive the constitutive relationship (expressed by ODEs) between stress and strain in frozen soil, using data from a coal mine in Huainan, China, measured by [51]. In [51], the fractional Kelvin model successfully characterized this constitutive relationship, expressed as

$$\frac{d^\alpha \varepsilon}{dt^\alpha} + \frac{E}{\eta} \varepsilon = \frac{\sigma}{\eta}, \quad (15)$$

where ε and σ denote strain and stress, respectively, d^α/dt^α represents the Caputo derivative of fractional order α ($0 < \alpha < 1$), E is the elasticity modulus, and η is the viscosity coefficient. Two types of frozen soil, clay and silt, were tested with sample sizes of 56 and 43, respectively. Note that the sampling interval is uneven, and the data contains natural noise. To generate candidate terms for integer- or fractional-order derivatives, data denoising and interpolation at specified positions were necessary. For both datasets, 15 samples were used as the training set, with the remainder for prediction. Using the trained DNN, 400 equidistant reconstructed data points for sparse regression and five auxiliary nodes for each reconstructed points (to compute fractional derivatives) were generated. As illustrated in Figure 3, the dataset was effectively denoised, and auxiliary points required for computing fractional derivatives were arbitrarily prescribed. Time evolutionary $\varepsilon_t^{(\alpha)}$ involving fractional derivative is computed by G-J quadrature, and candidate library Θ is generated via automatic differentiation as follows:

$$\Theta = \left[1 \quad \varepsilon \quad \varepsilon_t \quad \varepsilon_{tt} \quad \varepsilon^2 \quad \varepsilon\varepsilon_t \quad \varepsilon_t\varepsilon_t \quad \varepsilon\varepsilon_{tt} \quad \varepsilon_t\varepsilon_{tt} \quad \varepsilon_{tt}\varepsilon_{tt} \right], \quad (16)$$

and the right-hand-side the of equation is $\varepsilon_t^{(\alpha)}$, whose parameter α is unknown and is optimized by Difference Evolution algorithm (DE), as in Table 1. The discovery results, detailed in Table 2, demonstrate that our algorithm successfully identified the fractional Kelvin model structure directly from experimental data, without prior knowledge of the structural form of the differential equations. The parameter estimation error for clay was lower than that for silt (see Table 2), likely due to (1) the sharper transition in the silt stress-strain curve, which provides less information for learning; (2) loss of accuracy in G-J quadrature due to insufficient quadrature points; (3) the cumulative error of stepwise optimization leads to the deviation of parameters. Improving the parameter optimization for FDEs discovery is a potential topic in the future work.

3.2. Discovering FADE from synthetic data

In this section, we assess the effectiveness of our method in identifying fractional partial differential equations, with the Fractional Advection-Diffusion Equation (FADE) chosen as the case study. FADE is a parsimonious model

Table 1: Stepwise approach for discovery of FDEs

Algorithm framework

Step 0: Initialization

0.1 Random initialize the fractional order $\alpha = \alpha_0$ and $\beta = \beta_0$.

0.2 Generate the library using a deep-learning based method for the prescribed α_0 and β_0

$$\text{orders for fractional derivatives: } \hat{u}_x^{(\alpha)}(x, t) = \sum_{i=1}^5 \omega_i \hat{u}(\zeta_i, t).$$

Step 1: Sparse regression to update vector ξ

1.1 Estimate the optimal coefficient vector ξ using the STRidge algorithm:

$$\hat{\xi} = \arg \min_{\xi} L(\alpha_0, \beta_0, \xi).$$

Step 2: Global optimization to update α and β

2.1 Update the fractional orders α and β using a global optimization algorithm:

$$(\hat{\alpha}, \hat{\beta}) = \arg \min_{(\alpha, \beta)} L(\alpha, \beta, \hat{\xi}).$$

2.2 Rebuild the library based on the updated $\hat{\alpha}$ and $\hat{\beta}$

Step 3: Alternating direction optimization iteration

3.1 Repeat steps 1 and 2 until the loss function converges to a minimum, or the maximum number of iterations is reached.

Output: Return the optimized α , β , and ξ .

that captures anomalous solute diffusion in aquifers [32]. The mechanisms underlying FADEs vary depending on whether the fractional derivatives relate to time or space: FADEs with time fractional derivatives model delayed transport due to solute retention, while those with space fractional derivatives describe rapid solute displacement along preferential flow paths [52]. For generality, we examine FADE with both space and time fractional derivatives. To demonstrate the feasibility of our method in discovering FADE, synthetic data generated through numerical simulation of FADE is employed. The FADE and its initial and boundary conditions in this study are provided as follows:

$$\begin{cases} c_t^{(\alpha)} = -vc_x + Dc_x^{(\beta)}, \\ c(x, 0) = 10e^{-[(x-6)/10]^2}, \\ c(0, t) = c(30, t), \end{cases} \quad (17)$$

where $\alpha = 0.8$ and $\beta = 1.7$ denote the time and space fractional orders, respectively. A closed-form analytical solution has not yet been found, so we use the fast Fourier transform (FFT) to obtain $E_\alpha[(-iv\kappa + D(i\kappa)^\beta)t^\alpha]$, where κ represents the variable in frequency domain, and $E_\alpha(\cdot)$ denotes the single-parameter Mittag-Leffler function [38], expressed as

$$E_\alpha(z) = \sum_{n=0}^{\infty} \frac{z^n}{\Gamma(\alpha n + 1)}, \quad (18)$$

where α denotes the shape parameter, which represents the fractional order here. An inverse fast Fourier transform (IFFT) is then employed to obtain high-precision semi-analytical solutions, which serve as synthetic data. The candidate library constructed as

$$\Theta(\beta) = \left[1 \quad c \quad c_x \quad c_x^{(\beta)} \quad c_{xxx} \quad c^2 \quad cc_x \quad cc_{xx} \quad cc_{xxx} \quad c^2c_x \quad c^2c_{xx} \quad c^2c_{xxx} \right], \quad (19)$$

and the right-hand-side of equation is temporal fractional derivative $c_t^{(\alpha)}$. Generally, the advection term of solute transport is usually characterized by spatial gradient of concentration, which is first-order derivative, so we assume

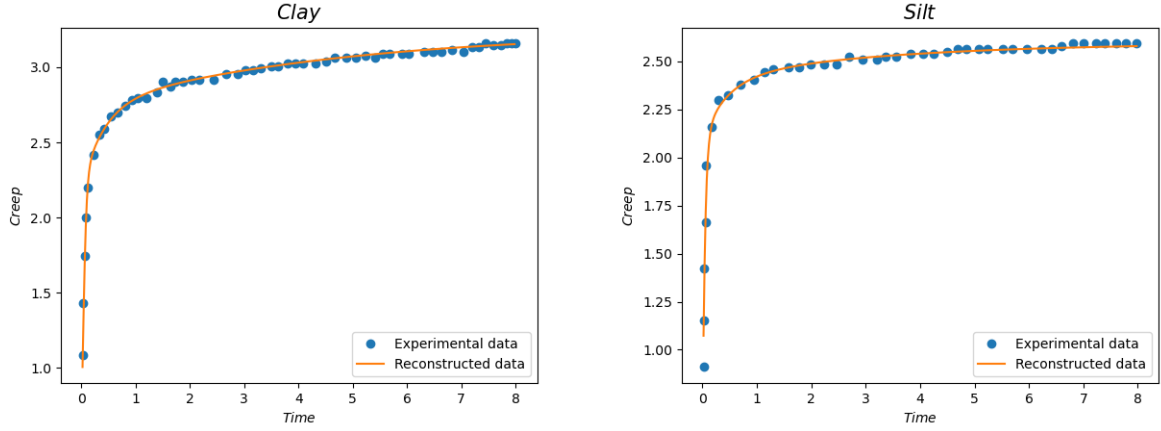


Figure 3: Reconstruction of experimental data for clay and silt.

Table 2: Summary of fractional Kelvin model learned from experimental data

Soil type		Equation	α	η	E	Error
Clay	Learned model	$\varepsilon_t^{(0.374)} = -2.402\varepsilon + 8.125$	0.374	0.137	0.328	0.151
	Ground truth	$\varepsilon_t^{(0.371)} = -3.010\varepsilon + 10.745$	0.371	0.103	0.320	/
Silt	Learned model	$\varepsilon_t^{(0.448)} = -7.344\varepsilon + 18.955$	0.448	0.0612	0.449	0.256
	Ground truth	$\varepsilon_t^{(0.562)} = -5.681\varepsilon + 14.910$	0.562	0.0778	0.442	/

¹ The "Error" in the table represents average relative error between the learned and ground truth parameters.

² The ground truth are obtained using the nonlinear least squares method to determine parameters, given that the model structure is predefined.

the order of derivative for advection to be an integer. The fractional orders α and β are optimized by DE algorithm, as in Table 1. The distribution of synthetic data at various noise levels and the corresponding reconstructed data are illustrated in Figure 4. Note that even clean data also requires reconstruction for computing fractional derivatives. The spatial and temporal scopes are $x = [0, 30]$ and $t = [0, 15]$, with a resolution of $(x \times t) = (120 \times 150) = 18000$, the time and space intervals are set uniformly to meet the requirements of the FFT-based algorithm. In this study, we consider three noise levels, namely clean (no noise), 5% uniform noise and 25% uniform noise. For clean data and 5% noisy data, we randomly select 1000 samples for training set and 2000 for the validation set, respectively. For 25% noise data, 1000 training points are insufficient for reliable reconstruction, so 2000 points are chosen for training set and validation set. Choosing the right training sample size is an important issue that deserves thorough research, as it involves the trade-off between researchers' workload and the accuracy of data reconstruction [10]. However, to keep the focus on the main topic of data-driven discovery of fractional differential equations, we have decided not to explore this issue systematically in this study.

The results of FDE discovery are summarized in Table 3. Our method successfully recovers the correct structure of FADE from synthetic data across various noise levels, though the accuracy of parameter estimation (including spatiotemporal fractional orders, velocity and diffusion coefficient) decreases as noise level increases, as indicated by a rise in mean squared error. This accuracy decline likely results from challenges in data reconstruction under high noise conditions. As noise increases, the fidelity of data reconstruction relative to clean data diminishes, preventing the loss function from accurately reflecting the original parameters of FADE.

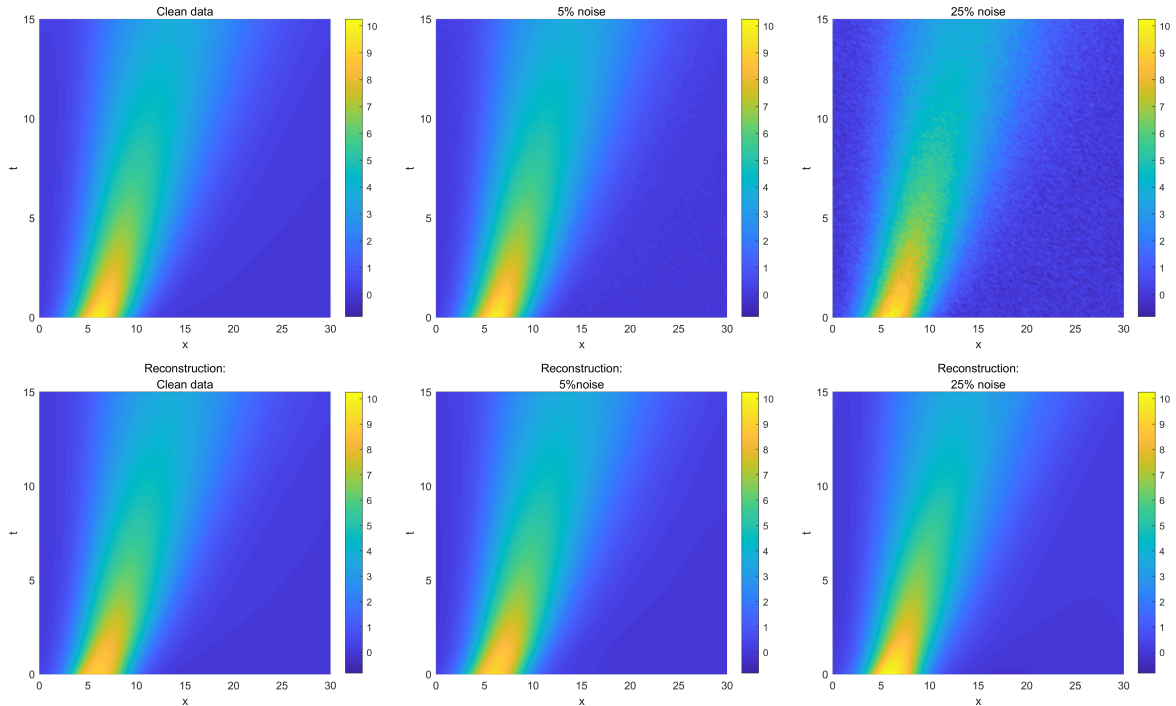


Figure 4: The upper panel illustrates the spatiotemporal distribution of synthetic data, governed by a fractional advection-diffusion equation, under varying noise levels. The lower panel shows the reconstructed data for the upper panel, generated using a DNN.

Table 3: Summary of FADE learned from noisy synthetic data

Noise level	Learned Equation	Error
Clean data	$c_t^{(0.790)} = -1.006c_x + 0.501c_x^{(1.720)}$	0.008
5% noise	$c_t^{(0.791)} = -1.005c_x + 0.510c_x^{(1.667)}$	0.014
25% noise	$c_t^{(0.804)} = -0.946c_x + 0.462c_x^{(1.750)}$	0.041
Ground truth	$c_t^{(0.8)} = -c_x + 0.5c_x^{(1.7)}$	-

3.3. Data-driven derivation of Stable Laws

The previous study has demonstrated success in data-driven discovery of diffusion equations from Brownian motion [6]. According to the central limit theorem, random walks with probability density function (PDF) in jump sizes characterized by finite mean and variance (such as Brownian motion), converge to a Gaussian distribution. However, in complex systems where the temporal-spatial distribution of random walker velocities exhibits a long-tail (i.e., power-law) property, this convergence does not hold. Under these conditions, particle trajectories cannot be accurately described by standard second-order diffusion equation. For example, Lévy motions, which are memoryless process characterized by finite mean displacement and divergent displacement variance, result in position densities that converges to the fractional diffusion equation based on the generalized central limit theory [53, 54]. Consider a random walk for Lévy motions

$$Y = X_1 + X_2 + \dots + X_n, \quad (20)$$

where the random variable Y represents the location after n jumps, and X denotes the independent and identically distributed (i.i.d.) jump lengths following an α -stable distribution $p(X) = S_\alpha(\beta, \sigma, \mu)$ [55] with parameters $1 < \alpha \leq 2$,

$-1 \leq \beta \leq 1$, $\sigma > 0$ and μ representing the shape factor, skewness, scale factor and drift, respectively. This random walk describes n jumps of a single particle with a constant time interval Δt between two consecutive jumps is constant.

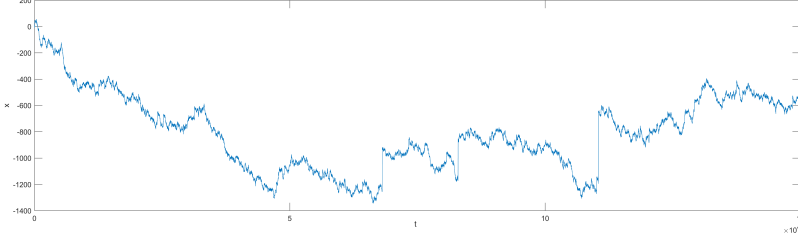


Figure 5: Single particle trajectory of Lévy motions.

When $\beta = 1$, $\sigma = (\Delta t D |\cos(\pi\alpha/2)|)^{1/\alpha}$ and $\mu = v\Delta t + \sigma\beta \tan(\pi\alpha/2)$ as $n \rightarrow \infty$, the random variable Y in Equation (20) may converge to a Stable Law (see Appendix B). The probability density function of Y is

$$p_Y(x, t) = S_\alpha(1, (Dt|\cos(\pi\alpha/2)|)^{1/\alpha}, vt + \sigma\beta \tan(\pi\alpha/2)), \quad (21)$$

which corresponds to the solution of the space-fractional diffusion equation (Appendix B)

$$\frac{\partial c(x, t)}{\partial t} = -v \frac{\partial c(x, t)}{\partial x} + D \frac{\partial^\alpha c(x, t)}{\partial x^\alpha} \quad (22)$$

where v represents the mean velocity of forward movement, and D is the effective dispersion coefficient, see Appendix B for more details. Notably, Gulian et al. [56] successfully learned fractional diffusion equations from α -stable time series by using Gaussian regression, though this approach relies on the availability of the structural form of the equation. The primary objective of this section is to discover the fractional differential equation without relying on any prior information, including its structural form, building on the work of [56]. The candidate library is identical to that in Section 3.2.

We consider a stable time series $S_{1.8}(1, 0.66, -0.32)$ with results presented in Table 4. The trajectory of this random walker is shown in Figure 5. The results demonstrate that a fractional diffusion equation has been successfully identified from the trajectory, the learned fractional orders for time and space are 0.987 and 1.842, respectively, with a diffusion coefficient of 0.475 (Table 4). Note that the temporal order learned by our algorithm closely approximates the true derivative order of one. This indicates that our framework is not limited to extracting FDEs; it can also effectively capture memoryless processes characterized by integer-order temporal derivatives through precise parameter calibration via global optimization.

Table 4: Summary of fractional diffusion model learned with α -stable time series

	Learned Equation	Error
Learned model	$c_t^{(0.987)} = 0.475 c_{xx}^{(1.842)}$	0.029
Ground truth	$c_t = 0.5 c_{xx}^{(1.8)}$	/

4. Discussion

4.1. Method comparison

To the best of our knowledge, our method is the first to directly extract FDEs from data without relying on any prior knowledge. To further prove the advancements of our method in discovering FDEs, we compare it with a representative PDE discovery framework, DL-PDE [10], which has shown robust performance in discovering many classical PDEs. The candidate library of DL-PDE is restricted to integer-order derivative terms, and it lacks an

optimization process for identifying fractional orders. The FADE described in Section 3.2 is used as the benchmark for this comparison.

The candidate library in DL-PDE is similar to that in our method, except it contains only integer-order derivative terms

$$\Theta = \left[1 \quad c \quad c_x \quad c_{xx} \quad c_{xxx} \quad c^2 \quad cc_x \quad cc_{xx} \quad cc_{xxx} \quad c^2c_x \quad c^2c_{xx} \quad c^2c_{xxx} \right]. \quad (23)$$

Compared to the candidate library in (19), the difference is DL-PDE replacing the second-order derivative terms with spatial fractional-order derivative terms. The comparison results are shown in Table 5. From Table 5, when applied to clean data, DL-PDE performs well in capturing specific physics characterized by first- and second-order terms, that is advection and local dispersion. The identified orders are the integer closest to the corresponding fraction of ground truth, and the corresponding coefficients exhibiting reasonable accuracy. However, it fails to extract fractional-order derivatives. Under noisy conditions, with 5% and 25% uniform noise, DL-PDE is limited to identifying second-order and first-order spatial derivatives, respectively, while demonstrating poor performance in coefficient regression. These findings indicate that DL-PDE is not suitable for discovering FDEs, although it can capture specific characteristics of dispersive transport, such as the mean flow rate (first-order derivative) and deviations from the mean flow rate (second-order derivative).

According to the comparison, our method demonstrates the irreplaceable ability to discover the correct fractional-order of FADE and its coefficients with relatively high accuracy.

Table 5: Comparison of FADE between our method and DL-PDE

Noise level	Our framework	DL-PDE
Clean data	$c_t^{(0.790)} = -1.006c_x + 0.501c_x^{(1.720)}$	$c_t = -0.964c_x + 0.416c_{xx}$
5% noise	$c_t^{(0.791)} = -1.005c_x + 0.510c_x^{(1.667)}$	$c_t = 1.270c_{xx}$
25% noise	$c_t^{(0.804)} = -0.946c_x + 0.462c_x^{(1.750)}$	$c_t = -0.569c_x$
Ground truth	$c_t^{(0.8)} = -c_x + 0.5c_x^{(1.7)}$	

4.2. The effect of regularization

Our method employs l_0 -regularization with a regularization factor λ (refer to Equation (14)) to achieve an effective balance between model parsimony and accuracy in the discovered equations. Particularly, the appropriate setting of λ is crucial for accurately identifying the governing equations (especially in terms of their structure). To determine the suitable magnitudes of λ within our framework, we perform a series of numerical experiments on the FADE model under three levels of noise (see also in Section 3.2). Four different magnitudes of regularization coefficients are considered: $\lambda = 10^{-5}$, $\lambda = 10^{-4}$, $\lambda = 10^{-3}$, and $\lambda = 10^{-2}$. The comparison results of discovered structures are shown in Table 6.

Table 6: The structural form of FADE under different levels of noise and different values of λ

λ	Clean data	5% noise	25% noise
10^{-5}	$c_t^{(0.790)}, c_x, c_x^{(1.720)}$	$c_t^{(0.811)}, c_x, c_x^{(1.597)}, c_{xxx}$	$c_t^{(0.828)}, c, c_x, c_x^{(1.916)}, c_{xxx}, c^2, cc_{xx}, cc_{xxx}$
10^{-4}	$c_t^{(0.796)}, c_x, c_x^{(1.641)}$	$c_t^{(0.791)}, c_x, c_x^{(1.667)}$	$c_t^{(0.832)}, 0.0371, c_x, c^2, c^2c_{xxx}$
10^{-3}	$c_t^{(0.795)}, c_x, c_x^{(1.610)}$	$c_t^{(0.802)}, c_x, c_x^{(1.608)}$	$c_t^{(0.804)}, c_x, c_x^{(1.750)}$
10^{-2}	$c_t^{(0.687)}, c_x$	$c_t^{(0.684)}, c_x$	$c_t^{(0.716)}, c_x$
Ground truth	$c_t^{(0.8)}, c_x, c_x^{(1.7)}$		

As shown in Table 6, although smaller λ may increase the accuracy of coefficient identification (i.e., fractional order), some redundant terms are identified due to the overfitting of sparse regression when λ is small. For example,

when $\lambda = 10^{-5}$, the discovered equation under 5% noise includes the term c_{xxx} , which is absent in the ground truth. On the other hand, increasing λ appropriately helps preserve model parsimony, but excessively large value of λ makes the model overly parsimonious, resulting in the lack of key terms in the discovered equation. For instance, when $\lambda = 10^{-2}$, the discovered equation lacks the spatial fractional derivative term $c_x^{(1.7)}$ compared to the ground truth. Moreover, the suitable range of λ varies with the noise intensity.

Furthermore, the suitable range of λ varies with the noise intensity. For instance, with clean data, $\lambda = 10^{-5}$ yields a discovered equation consistent with the ground truth, while under 5% and 25% noise, it contains one and five redundant terms, respectively. Similarly, when $\lambda = 10^{-4}$, the discovered equation is consistent with the ground truth for clean data and 5% noise, but under 25% noise, it contains three false terms. This indicates that lower noise levels allow for a broader range of optimal λ . In summary, $\lambda = 10^{-3}$ is the most practical choice for FDE discovery, as it successfully identifies the correct structural form of the FADE and its parameters under various noise levels.

5. Conclusions

In this study, we present a stepwise framework for identifying fractional differential equations (FDEs) directly from data. We validate our approach by recovering commonly-used FDEs across three scenarios: experimental data of frozen soil creep behavior, synthetic data of solute transport in aquifers, and a single particle trajectory of Lévy motion. These case studies demonstrate that our algorithm effectively extracts practical FDEs, showing robustness across various levels of natural and artificial noise. The algorithm integrates both fractional-order and integer-order derivatives into the candidate library, broadening its scope of applicability. Moreover, memoryless dynamics can be captured by calibrating the fractional order to approximate integer values. To further validate the advancements of our framework in identifying FDEs, a comparative analysis with a representative existing method, DL-PDE, is conducted. Additionally, the applicable range of the regularization factor for different levels of data noise is analyzed. The results indicate that as noise intensity decreases, the range of suitable regularization values broadens. And $\lambda = 10^{-3}$ falls within the optimal range across different noise levels.

The current approach remains several limitations. Firstly, the proposed framework is relatively time-consuming, requiring multiple steps to optimize different parameter groups. Future work could focus on developing a more efficient algorithm to reduce the computational cost of the proposed framework. Secondly, although the method performs robustly in discovering the correct structure of FDEs, the accuracy of parameter estimation is limited likely due to the data quality and the optimization algorithm's capabilities. In some cases (e.g., contaminant transport in groundwater), sample availability is extremely limited due to challenging data acquisition in complex systems, and high noise intensity. Future work could focus enhancing the algorithm to effectively discover FDEs from highly sparse and noisy data. Finally, besides the FDEs in this study, there is a wide spectrum of parsimonious models aimed at capturing different mechanisms that play important roles in the dynamics of complex systems. Discovering these models could be a promising direction for future work. To achieve this goal, a large, closed library that encompassed all possible candidate terms for describing the dynamics of complex systems is required, which is unrealistic. Improving the flexibility of our algorithm by reducing the reliance on overcomplete candidate library offers promising solutions to this challenge, for example, adopting expandable libraries [57] or using open-formed algorithms [21].

Acknowledgement

The codes and datasets for this research is available when this manuscript is accepted.

Appendix A. Gaussian-Jacobi quadrature

Due to their nonlocal and singular nature, approximating fractional derivatives presents numerical challenges. Nonlocality increases computational cost, particularly at large time or space scales, as it requires dividing the computation region into a fine unit grid. To address this issue, we employ Gaussian-Jacobi (G-J) quadrature, an effective method for integrands with endpoint singularities. G-J quadrature is a refined numerical integration technique that provides accurate approximations for integrals with power-law weight functions like $(1-x)^{\mu}(1+x)^{\nu}$. The general quadrature formula is as follows

$$\int_{-1}^{+1} f(x)\rho^{(\mu,\lambda)}(x)dx = \sum_{i=1}^N \omega_i f(\xi_i), \quad (\text{A.1})$$

where $\rho^{(\mu,\lambda)} = (1-x)^\lambda(1+x)^\mu$ denotes the singular kernel function, and ω_i represents weight factors determined by G-J rule, as referenced in [58], N denotes the prescribed number of quadrature nodes. The quadrature nodes, denoted by ξ , are associated with the weight factors ω_i , both of which can be determined using the Golub-Welsch algorithm or, alternatively, by directly using SciPy Python package, which includes this algorithm. The G-J rule efficiently computes the fractional integral of any smooth function. By substituting $\epsilon(\tau) = (t-a)(1+\tau)/2$, Equation (4) can be rewritten as

$$I_a^\gamma f(t) = \frac{(t-a)^\gamma}{\Gamma(\gamma)} \int_{-1}^1 (1+\tau)^{\gamma-1} f[\epsilon(t,\tau)]d\tau, \quad (\text{A.2})$$

which can be regarded as the Gaussian-Jacobi quadrature (A.1) with $\mu = 0$ and $\lambda = \gamma - 1$. The fractional derivatives can then be obtained using Equations (2) and (3). The G-J rule's ability to handle singular integrals is a crucial advantage in solving fractional differential equations, enabling effective and accurate solutions. This approach allows us to embed the fractional derivative term into the candidate library, resulting in solving this system, we obtain approximate solutions that accurately capture the behavior of fractional differential equations, even in the presence of singularities.

We examine the example $\frac{d^{4/5}t^{1/2}}{dt^{4/5}}$, using the Caputo definition of the fractional derivative. The exact solution is given by $\Gamma(1.5)t^{-0.3}/\Gamma(2.3)$, highlighting the singularity at the origin. We compare the numerical performance of the finite difference method (FDM) [59] and G-J quadrature. As shown in Figure A.6, the inherent singularity in fractional derivatives results in insufficient accuracy for FDM, and precision does not improve (see Table A.7) as the temporal grid Δt decreases from 0.1 (Fig. A.6a) to 0.01 (Fig. A.6b). Accuracy is particularly low near the origin. In contrast, the G-J quadrature method achieves a high precision with only five quadrature points, and performs well at the origin. Moreover, With higher accuracy, G-J quadrature is more efficient than the finite difference method (Table A.7). Thus, G-J quadrature outperforms FDM, especially in scenario where singularities exist.

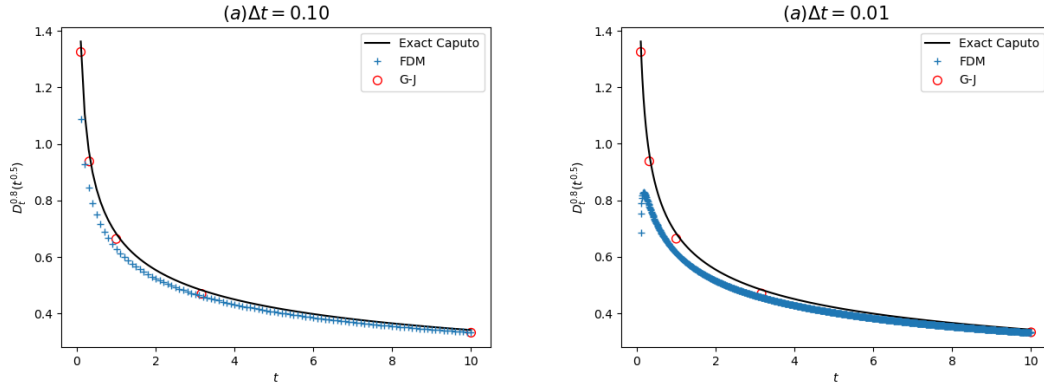


Figure A.6: Comparison of differentiation strategies, finite difference method (FDM) versus Gaussian-Jacobi quadrature (G-J) for fractional derivatives.

Appendix B. Stable Law

Appendix B.1. Stable distribution

The probability density function of a stable distribution has no explicit formula; it is represented by its Fourier transform [60]

Table A.7: Time cost and precision of Gaussian-Jacobi quadrature and finite difference method

	CPU time (s)	l_2 -error
FDM ($\Delta t = 0.1$)	0.0081	17.35
FDM ($\Delta t = 0.01$)	0.78	163.19
G-J	0.00028	1.85

* The number of G-J nodes is five and remains independent of the time interval Δt .

$$\hat{p}(k) = \exp[-|k|^\alpha \sigma^\alpha (1 + i\beta \text{sign}(k) \tan(\pi\alpha/2) - \mu ik)] \quad (\text{B.1})$$

where $0 < \alpha \leq 2$, $\sigma > 0$, $-1 \leq \beta \leq 1$, and μ represent the shape, scale, skewness and drift respectively. Setting $\sigma = (C|\cos(\pi\alpha/2)|)^{1/\alpha}$ and $\beta = p - q$, where C is a positive parameter and $p + q = 1$, we obtain the equivalent form [54]

$$\hat{p}(k) = \exp[qC(-ik)^\alpha + pC(ik)^\alpha - \mu ik]. \quad (\text{B.2})$$

Particularly, when $\beta = 1$ (i.e., $p = 1$ and $q = 0$), $\mu = v$ and $C = Dt$, the function in $\hat{p}(k)$ in (B.2) is equal to the function (21), which is the solution to the space fractional advection-diffusion (22) under the application of the Fourier transform.

Appendix B.2. Lévy motion

Now consider the Langevin equation for single particle motion

$$dX(t) = Vdt + BdL_\alpha(t). \quad (\text{B.3})$$

Following the detailed study by [61], when $V = v$, $B = [D|\cos(\pi\alpha/2)|]^{1/\alpha}$ and $dL_\alpha(t) = (dt)^{1/\alpha} S_\alpha(\beta = 1, \sigma = 1, \mu = 0)$, the particle number density for Equation (B.3) satisfies the space-fractional advection-diffusion equation (22). By coarse-graining the Langevin equation (B.3) with $\Delta t \approx dt$, we obtain

$$X(t_{i+1}) = X(t_i) + V\Delta t + B\Delta t^{1/\alpha} S_\alpha(\beta = 1, \sigma = 1, \mu = 0), \quad (\text{B.4})$$

where $\Delta t = t_{i+1} - t_i$ and $i = 1, 2, \dots, n$. According to the parameterization law by [62], $X(t)$ follows

$$X(t_{i+1}) = X(t_i) + S_\alpha(1, \sigma, v\Delta t + \sigma\beta \tan(\pi\alpha/2)), \quad (\text{B.5})$$

where $\sigma = (\Delta t D |\cos(\pi\alpha/2)|)^{1/\alpha}$. The recursion for the random variable X in Equation (B.5) represents the Lévy motion (20), which is equivalent to the space FADE (22). Thus, the Lévy motion (20) can be considered a coarse-grained representation of the Markov process (B.3), whose scale limit is the space FADE (22).

References

- [1] Steven L Brunton and J Nathan Kutz. Promising directions of machine learning for partial differential equations. *Nature Computational Science*, pages 1–12, 2024. Publisher: Nature Publishing Group US New York.
- [2] John R Koza. Genetic programming as a means for programming computers by natural selection. *Statistics and Computing*, 4:87–112, 1994.
- [3] Josh Bongard and Hod Lipson. Automated reverse engineering of nonlinear dynamical systems. *Proceedings of the National Academy of Sciences*, 104(24):9943–9948, 2007. Publisher: National Acad Sciences.
- [4] Michael Schmidt and Hod Lipson. Distilling free-form natural laws from experimental data. *Science*, 324(5923):81–85, 2009.
- [5] Steven L Brunton, Joshua L Proctor, and J Nathan Kutz. Discovering governing equations from data by sparse identification of nonlinear dynamical systems. *Proceedings of the National Academy of Sciences*, 113(15):3932–3937, 2016.
- [6] Samuel H Rudy, Steven L Brunton, Joshua L Proctor, and J Nathan Kutz. Data-driven discovery of partial differential equations. *Science Advances*, 3(4):e1602614, 2017. Publisher: American Association for the Advancement of Science.
- [7] Haibin Chang and Dongxiao Zhang. Machine learning subsurface flow equations from data. *Computational Geosciences*, 23(5):895–910, 2019.

- [8] Daniel A Messenger and David M Bortz. Weak sindy for partial differential equations. *Journal of Computational Physics*, 443:110525, 2021.
- [9] Urban Fasel, J Nathan Kutz, Bingni W Brunton, and Steven L Brunton. Ensemble-sindy: Robust sparse model discovery in the low-data, high-noise limit, with active learning and control. *Proceedings of the Royal Society A*, 478(2260):20210904, 2022.
- [10] Hao Xu, Haibin Chang, and Dongxiao Zhang. Dl-pde: Deep-learning based data-driven discovery of partial differential equations from discrete and noisy data. *arXiv preprint arXiv:1908.04463*, 2019.
- [11] Gert-Jan Both, Subham Choudhury, Pierre Sens, and Remy Kusters. Deepmod: Deep learning for model discovery in noisy data. *Journal of Computational Physics*, 428:109985, 2021.
- [12] Maziar Raissi, Paris Perdikaris, and George E Karniadakis. Physics-informed neural networks: A deep learning framework for solving forward and inverse problems involving nonlinear partial differential equations. *Journal of Computational Physics*, 378:686–707, 2019.
- [13] Yuntian Chen and Dongxiao Zhang. Integration of knowledge and data in machine learning. *arXiv preprint arXiv:2202.10337*, 2022.
- [14] Hao Xu and Dongxiao Zhang. Robust discovery of partial differential equations in complex situations. *Physical Review Research*, 3(3):033270, 2021.
- [15] R. Metzler and J. Klafter. The random walk’s guide to anomalous diffusion: a fractional dynamics approach. *Physics Reports*, 339(1):1–77, 2000.
- [16] Alessandro Comolli, Vivien Hakoun, and Marco Dentz. Mechanisms, upscaling, and prediction of anomalous dispersion in heterogeneous porous media. *Water Resources Research*, 55(10):8197–8222, 2019.
- [17] Samuel Rudy, Alessandro Alla, Steven L Brunton, and J Nathan Kutz. Data-driven identification of parametric partial differential equations. *SIAM Journal on Applied Dynamical Systems*, 18(2):643–660, 2019.
- [18] Stephen W. Wheatcraft and Scott W Tyler. An explanation of scale-dependent dispersivity in heterogeneous aquifers using concepts of fractal geometry. *Water Resources Research*, 24(4):566–578, 1988. Publisher: Wiley Online Library.
- [19] Peter Salamon, Daniel Fernández-García, and J Jaime Gómez-Hernández. A review and numerical assessment of the random walk particle tracking method. *Journal of Contaminant Hydrology*, 87(3-4):277–305, 2006.
- [20] Hao Xu, Dongxiao Zhang, and Nanzhe Wang. Deep-learning based discovery of partial differential equations in integral form from sparse and noisy data. *Journal of Computational Physics*, 445:110592, 2021.
- [21] Yuntian Chen, Yingtao Luo, Qiang Liu, Hao Xu, and Dongxiao Zhang. Symbolic genetic algorithm for discovering open-form partial differential equations (sga-pde). *Physical Review Research*, 4(2):023174, 2022.
- [22] Mengge Du, Yuntian Chen, and Dongxiao Zhang. Discover: Deep identification of symbolically concise open-form partial differential equations via enhanced reinforcement learning. *Physical Review Research*, 6(1):013182, 2024.
- [23] Mengge Du, Longfeng Nie, Siyu Lou, Yuntian Chen, and Dongxiao Zhang. Physics-constrained robust learning of open-form pdes from limited and noisy data. *arXiv preprint arXiv:2309.07672*, 2023.
- [24] Mengge Du, Yuntian Chen, Zhongzheng Wang, Longfeng Nie, and Dongxiao Zhang. Llm4ed: Large language models for automatic equation discovery. *arXiv preprint arXiv:2405.07761*, 2024.
- [25] Alexandre M Tartakovsky, C Ortiz Marrero, Paris Perdikaris, Guzel D Tartakovsky, and David Barajas-Solano. Physics-informed deep neural networks for learning parameters and constitutive relationships in subsurface flow problems. *Water Resources Research*, 56(5):e2019WR026731, 2020.
- [26] Keith Beven and Jim Freer. Equifinality, data assimilation, and uncertainty estimation in mechanistic modelling of complex environmental systems using the glue methodology. *Journal of Hydrology*, 249(1-4):11–29, 2001.
- [27] E Eric Adams and Lynn W Gelhar. Field study of dispersion in a heterogeneous aquifer: 2. spatial moments analysis. *Water Resources Research*, 28(12):3293–3307, 1992.
- [28] John H. Cushman, Lynn S. Bennethum, and Bill X Hu. A primer on upscaling tools for porous media. *Advances in Water Resources*, 25(8-12):1043–1067, 2002. Publisher: Elsevier.
- [29] Shlomo P. Neuman. Universal scaling of hydraulic conductivities and dispersivities in geologic media. *Water Resources Research*, 26(8):1749–1758, 1990.
- [30] Gedeon Dagan. Theory of solute transport by groundwater. *Annual Review of Fluid Mechanics*, 19(1):183–213, 1987.
- [31] Brian Berkowitz, Andrea Cortis, Marco Dentz, and Harvey Scher. Modeling non-fickian transport in geological formations as a continuous time random walk. *Reviews of Geophysics*, 44(2), 2006.
- [32] David A Benson, Stephen W Wheatcraft, and Mark M Meerschaert. Application of a fractional advection-dispersion equation. *Water Resources Research*, 36(6):1403–1412, 2000.
- [33] Roy Haggerty and Steven M Gorelick. Multiple-rate mass transfer for modeling diffusion and surface reactions in media with pore-scale heterogeneity. *Water Resources Research*, 31(10):2383–2400, 1995.
- [34] Nicholas Geneva and Nicholas Zabararas. Quantifying model form uncertainty in reynolds-averaged turbulence models with bayesian deep neural networks. *Journal of Computational Physics*, 383:125–147, 2019.
- [35] Markus Schöberl, Nicholas Zabararas, and Phaedon-Stelios Koutsourelakis. Predictive coarse-graining. *Journal of Computational Physics*, 333:49–77, 2017.
- [36] Joseph Bakarji and Daniel M Tartakovsky. Data-driven discovery of coarse-grained equations. *Journal of Computational Physics*, 434:110219, 2021.
- [37] Anatoliĭ Aleksandrovich Kilbas, Hari M Srivastava, and Juan J Trujillo. *Theory and applications of fractional differential equations*, volume 204. elsevier, 2006.
- [38] I. Podlubny. *Fractional Differential Equations*. Academic Press, 1999.
- [39] Mark M Meerschaert and Alla Sikorskii. *Stochastic models for fractional calculus*, volume 43. Walter de Gruyter GmbH & Co KG, 2019.
- [40] Boling Guo, Xueke Pu, and Fenghui Huang. *Fractional partial differential equations and their numerical solutions*. World Scientific, 2015.
- [41] HongGuang Sun, Yong Zhang, Dumitru Baleanu, Wen Chen, and YangQuan Chen. A new collection of real world applications of fractional calculus in science and engineering. *Communications in Nonlinear Science and Numerical Simulation*, 64:213–231, 2018.
- [42] HongGuang Sun, Yong Zhang, Song Wei, Jianting Zhu, and Wen Chen. A space fractional constitutive equation model for non-newtonian fluid flow. *Communications in Nonlinear Science and Numerical Simulation*, 62:409–417, 2018.

- [43] H Schiessel, R Metzler, A Blumen, and TF Nonnenmacher. Generalized viscoelastic models: their fractional equations with solutions. *Journal of Physics A: Mathematical and General*, 28(23):6567, 1995.
- [44] Enrico Scalas, Rudolf Gorenflo, and Francesco Mainardi. Fractional calculus and continuous-time finance. *Physica A: Statistical Mechanics and its Applications*, 284(1-4):376–384, 2000.
- [45] Zongze Yang, Jungang Wang, Zhanbin Yuan, and Yufeng Nie. Using gauss-jacobi quadrature rule to improve the accuracy of fem for spatial fractional problems. *Numerical Algorithms*, pages 1–23, 2022.
- [46] Guofei Pang, Wen Chen, and Kam-Yim Sze. Gauss-jacobi-type quadrature rules for fractional directional integrals. *Computers & Mathematics with Applications*, 66(5):597–607, 2013.
- [47] Guofei Pang, Lu Lu, and George Em Karniadakis. fpinns: Fractional physics-informed neural networks. *SIAM Journal on Scientific Computing*, 41(4):A2603–A2626, 2019.
- [48] Zhao Chen, Yang Liu, and Hao Sun. Physics-informed learning of governing equations from scarce data. *Nature Communications*, 12(1):6136, 2021.
- [49] Xingjian Xu and Minghua Chen. Discovery of subdiffusion problem with noisy data via deep learning. *Journal of Scientific Computing*, 92(1):23, 2022.
- [50] Maziar Raissi. Deep hidden physics models: Deep learning of nonlinear partial differential equations. *Journal of Machine Learning Research*, 19(25):1–24, 2018.
- [51] Junhao Chen, Zhaoming Yao, Ying Xu, and Houliang Wang. Particle swarm fractional order derivative model of artificial frozen soil creep properties. *Journal of China Coal Society*, 38(10):1763–1768, 2013.
- [52] Yong Zhang, David A Benson, and Donald M Reeves. Time and space nonlocalities underlying fractional-derivative models: Distinction and literature review of field applications. *Advances in Water Resources*, 32(4):561–581, 2009.
- [53] Boris Vladimirovich Gnedenko, Andrei Nikolaevich Kolmogorov, Joseph L Doob, and Pao-Lu Hsu. *Limit distributions for sums of independent random variables*, volume 233. Addison-wesley Reading, MA, 1968.
- [54] David A Benson, Rina Schumer, Mark M Meerschaert, and Stephen W Wheatcraft. Fractional dispersion, lévy motion, and the made tracer tests. *Transport in Porous Media*, 42(1):211–240, 2001.
- [55] Paul Lévy. *Théorie de l'addition des variables aléatoires*. Gauthier-Villars, 1954.
- [56] Mamikon Gulian, Maziar Raissi, Paris Perdikaris, and George Karniadakis. Machine learning of space-fractional differential equations. *SIAM Journal on Scientific Computing*, 41(4):A2485–A2509, 2019.
- [57] Hao Xu, Haibin Chang, and Dongxiao Zhang. Diga-pde: Discovery of pdes with incomplete candidate library via combination of deep learning and genetic algorithm. *Journal of Computational Physics*, 418:109584, 2020.
- [58] Jie Shen, Tao Tang, and Li-Lian Wang. *Spectral methods: algorithms, analysis and applications*, volume 41. Springer Science & Business Media, 2011.
- [59] Y. Lin and C. Xu. Finite difference/spectral approximations for the time-fractional diffusion equation. *Journal of Computational Physics*, 225(2):1533–1552, 2007.
- [60] William Feller. *An introduction to probability theory and its applications, Volume 2*, volume 81. John Wiley & Sons, 1991.
- [61] Yong Zhang, David A Benson, Mark M Meerschaert, and Hans-Peter Scheffler. On using random walks to solve the space-fractional advection-dispersion equations. *Journal of Statistical Physics*, 123:89–110, 2006.
- [62] John P Nolan. Parameterizations and modes of stable distributions. *Statistics & Probability Letters*, 38(2):187–195, 1998.